Check for updates

Angewandte Chemie International Edition

Angewandte International Edition Chemie

GDCh German Chemical Society

How to cite: *Angew. Chem. Int. Ed.* **2026**, e7481604
doi.org/10.1002/anie.7481604

RESEARCH ARTICLE

Regulating π–π Stacking Interactions to Boost Near-Infrared Light-Driven CO_2 Reduction

Chong-Jiu Lu | Xin-Yue Zheng | Yun-Nan Gong | Di-Chang Zhong | Tong-Bu Lu

Institute for New Energy Materials and Low Carbon Technologies, School of Materials Science and Engineering, Tianjin University of Technology, Tianjin, China

Correspondence: Yun-Nan Gong (yngong@email.tjut.edu.cn) | Di-Chang Zhong (dczhong@email.tjut.edu.cn)

Received: 11 December 2025 | **Revised:** 16 April 2026 | **Accepted:** 29 April 2026

Keywords: CO_2 photoreduction | near-infrared light | π frameworks | π–π stacking

ABSTRACT

Developing highly efficient photocatalysts to achieve near-infrared (NIR) light-driven CO_2 reduction is of great significance yet remains a great challenge. In this article, we found that BODIPY-based π frameworks can serve as good NIR photocatalysts, achieving highly efficient CO_2 reduction to $HCOO^-$ coupled with benzyl alcohol oxidation to benzaldehyde in pure water. More impressively, the photocatalytic performance of these π frameworks can be improved by regulating π–π stacking interactions, among which the optimized π-pyrenyl (π-PY) framework with the most π–π stacking interactions exhibits $HCOO^-$ production rates of 4045 and 1693 μmol g^{-1} h^{-1} in >99% and 15% CO_2 atmospheres, respectively. π-PY, thus, stands for the current state-of-the-art photocatalyst in NIR-light-driven CO_2 reduction. Experiments together with theoretical calculations demonstrated that the high photocatalytic activity of π-PY could be due to the abundant π–π stacking interactions, which accelerates charge separation and transfer, as well as prolongs carrier lifetime and reduces energy gap. This work gives new insights in understanding the contribution of π–π stacking interactions to photocatalysis, and introduces a new strategy for developing efficient photocatalysts for NIR-light-driven CO_2 reduction.

1 | Introduction

Amid growing energy demand and rapidly increasing carbon dioxide (CO_2) emission in the atmosphere, numerous carbon-neutral technologies have been developed to convert CO_2 to valuable chemical fuels [1–4]. Among them, solar-driven CO_2 reduction is widely regarded as a promising way to achieve carbon neutral goal due to its environment-friendly and low-cost [5–10]. Over the past decade, a large number of high-performance photocatalysts have been designed and synthesized to convert CO_2 into carbon monoxide (CO), methane (CH_4), and formic acid (HCOOH), etc. [11–15]. However, most of them can only drive CO_2 conversion at ultraviolet (UV) and/or visible light regions, the near-infrared (NIR) light-driven CO_2 reduction has been rarely reported [16–20]. This can be attributed to the low photon energy of NIR light, which is difficult to drive the uphill CO_2 reduction reaction. Considering the NIR light occupies over 50% of the solar spectrum, the development of efficient photocatalysts to realize NIR-light-driven CO_2 reduction, in spite of greatly challenging, is much desired [21–26].

Several strategies have been developed to promote NIR-light-driven CO_2 reduction reaction [27, 28]. For example, the construction of surface plasmon resonance composites to expand the light absorption region from UV/visible light to NIR light; the addition of up-conversion materials to transform low-energy photons into high-energy photons; the construction of heterojunctions to improve carrier separation efficiency, and so on [29–33]. Nevertheless, it is difficult to understand the structure–activity relationship by the above strategies due to the lack of well-defined structures of these composites. In this regard, it is very meaningful to develop photocatalysts with definite crystal

© 2026 Wiley-VCH GmbH

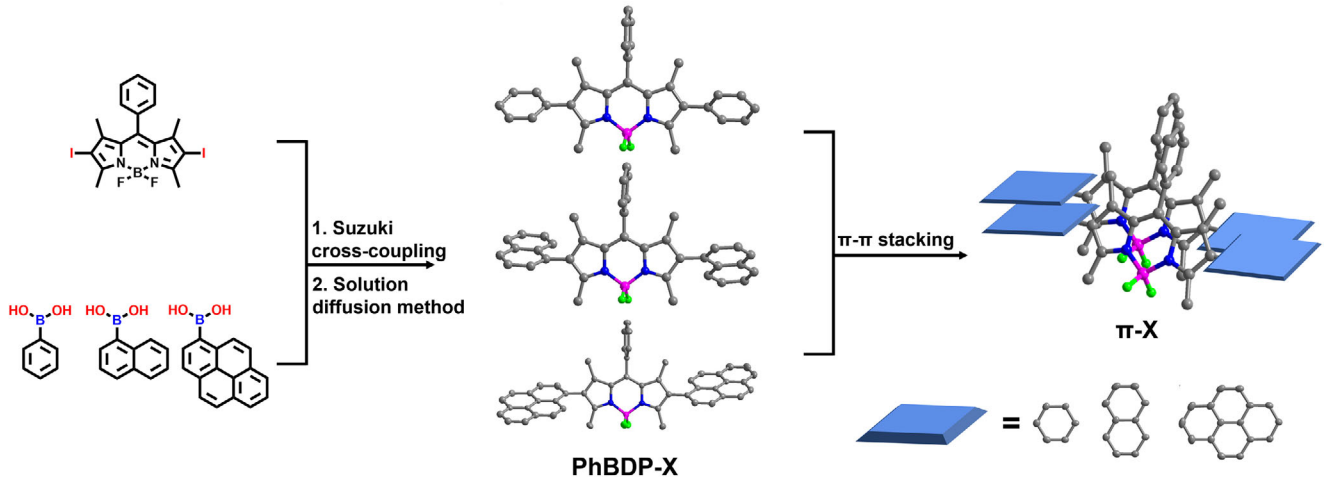

FIGURE 1 | Schematic of the synthesis of π-X frameworks (X = PY, Nap, and Ph).

structures for NIR-light-driven CO_2 reduction, which could get in-depth insights into the activity–structure relationship of the photocatalysts.

As a new class of porous crystalline materials, π frameworks assembled from functional molecules with conjugated groups through π–π stacking interactions, have shown potential application in many fields [34–37]. In particular, π frameworks exhibit unique characteristics in photocatalysis: 1) the large conjugated moieties give them excellent light harvesting ability for UV, visible and even NIR light; 2) the π–π stacking is an electron transfer channel, which can facilitate photo-induced electron delivery and thus boost photocatalysis; 3) the periodic and well-defined structures of π frameworks facilitate to deep understand the activity−structure relationship; 4) the weak noncovalent π–π stacking interactions in π frameworks make them easy healing and regeneration. With the above advantages, π frameworks are expected to be promising photocatalysts for NIR-light-driven CO_2 reduction [38, 39]. However, to our knowledge, the π frameworks were reported for photocatalytic reactions only by UV/visible light illumination [40, 41].

Herein, three PhBDP-based π frameworks with different π–π stacking interactions have been designed and synthesized, and were found for NIR-light-driven CO_2 reduction (Figure 1). Specifically, with dinuclear cobalt complex as the co-catalyst, they exhibit excellent NIR-light-driven catalytic activities for the reduction of CO_2 to $HCOO^-$, coupled with benzyl alcohol oxidation to benzaldehyde, among which the π-pyrenyl (π-PY) framework with 11 types of π–π stacking interactions displays the largest $HCOO^-$ production rates of 4045 μmol g^{-1} h^{-1}, which is ca. 2 and 12 times higher than the π-naphthyl (π-Nap) and π-phenyl (π-Ph) frameworks with 6 and 1 types of π–π stacking interactions, respectively. Moreover, π-PY shows a high $HCOO^-$ production rate of 1693 μmol g^{-1} h^{-1} for NIR-light-driven CO_2 reduction in low concentration (15%). The significantly enhanced photocatalytic performance of π-PY is attributed to the increased photo-induced electron transfer, prolonged carrier lifetime and reduced energy gap, as demonstrated by a series of photoelectrochemical experiments and theoretical calculations.

2 | Results and Discussions

The PhBDP-based compounds with different conjugated aromatic moieties (PhBDP-X, X = PY, Nap, and Ph; PhBDP = 5,5-difluoro-1,3,7,9-tetramethyl-10-phenyl-5H-4l4,5l4-dipyrrolo[1,2-*c*:2',1'-*f*][1,3,2]diazaborinine) were synthesized through the Suzuki cross-coupling reactions between PhBDP-I_2 and aromatic boronic acid compounds (Figure 1) [42]. The results of ^1H and ^{13}C nuclear magnetic resonance (NMR) spectra show that PhBDP-X were successfully obtained with high purity (Figures S1–S6). Afterward, the orange-red large-sized single crystals of π-X were obtained by slowly diffusing *n*-hexane into the dichloromethane solution of PhBDP-X at room temperature for 7 days (Figure 1). The results of single crystal x-ray diffraction analysis reveal that π-PY crystallizes in the orthorhombic system with $Pca2_1$ space group, and π-Nap and π-Ph crystallize in the monoclinic system with $P2_1/c$ and C_2/c space groups, respectively (Table S1). In π-X, adjacent PhBDP-X structural units are connected through strong π–π stacking interactions to form building blocks (Table S2). As shown in Figures 2a and S7, there are 11 types of π–π stacking interactions in π-PY, which are Cg1–Cg2, Cg3–Cg4, Cg3–Cg6, Cg4–Cg5, Cg4–Cg6, Cg5–Cg6, Cg8–Cg9, Cg8–Cg11, Cg9–Cg10, Cg9–Cg11, and Cg10–Cg11. For π-Nap, there are six types of π–π stacking interactions, which are Cg1–Cg10, Cg4–Cg7, Cg4–Cg15, Cg6–Cg16, Cg12–Cg14, and Cg13–Cg16 (Figure S8). For π-Ph, there is only one type of π–π stacking interaction (Cg1–Cg1; Figure S9). Neighboring building blocks are further linked via C—H···π hydrogen bonds to form three-dimensional (3D) stacked frameworks (Figures S7–S9 and Table S2). With increasing π–π stacking interactions, the distance of aromatic cores progressively decreases, accompanied by a reduction in the dihedral angle between adjacent aromatic planes, indicating the more coplanar and tightly packed arrangement. These may facilitate the charge separation and photogenerated electron transfer (Figures S7–S9). To characterize whether dimeric or higher-order aggregates formation occurs in π–π stacked frameworks, the NMR titration experiment was conducted. Taking π-PY as a representative example, the results of ^1H NMR indicate that no dimeric or higher-order aggregates are formed in π-PY (Figures S10–S13).

15213773, 0, Downloaded from https://onlinelibrary.wiley.com/doi/10.1002/anie.7481604 by Tianjin University Of Technology, Wiley Online Library on [29/05/2026]. See the Terms and Conditions (https://onlinelibrary.wiley.com/terms-and-conditions) on Wiley Online Library for rules of use; OA articles are governed by the applicable Creative Commons License

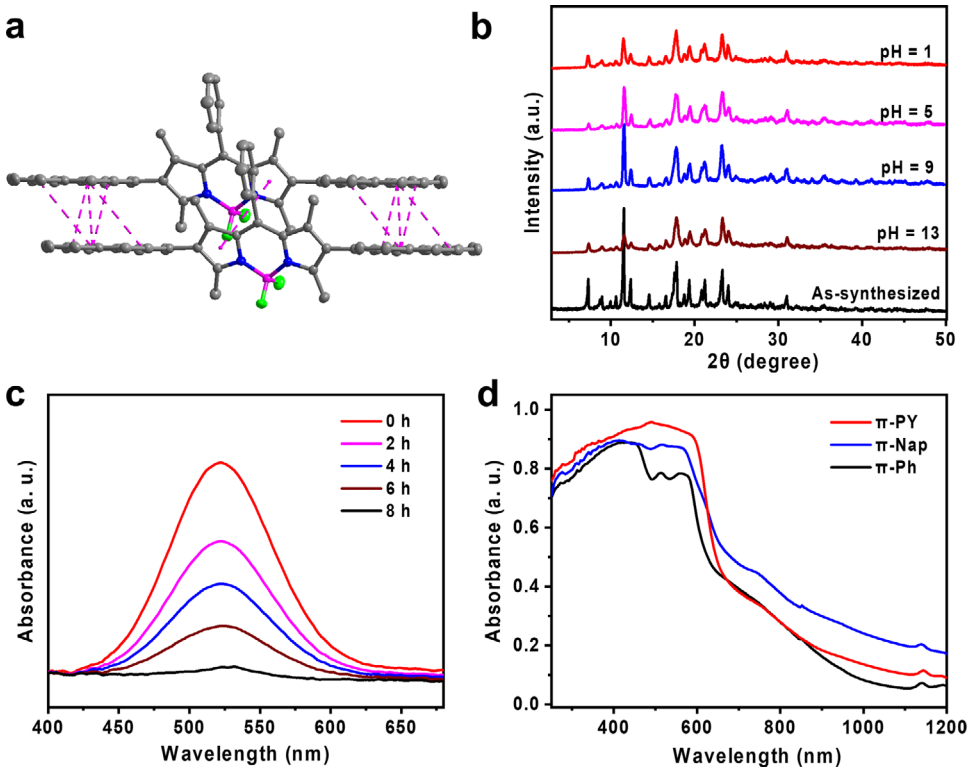

FIGURE 2 | (a) Schematic of 11 types of π–π stacking interactions in π-PY. (b) Powder XRD patterns of π-PY in aqueous solutions at pH 1–13 for 24 h. (c) UV–vis spectra of I_2 *n*-hexane solution where π-PY was soaked at given intervals. (d) The solid-state UV–vis-NIR spectra of π-X.

The results of powder x-ray diffraction (XRD) measurements show that the experimental patterns of π-X are basically consistent with the simulated ones, indicating their high phase purities (Figures S14–S16). Thermogravimetric analysis (TGA) curves of π-X demonstrate that they exhibit excellent thermal stability up to 300°C (Figures S17–S19). The chemical stability of π-X was further studied by soaking π-X in aqueous solutions with different pH values. The results of powder XRD measurements show that π-X exhibit exceptional stability, which can retain their framework integrity in aqueous solutions at pH 1–13 for over 24 h (Figures 2b, S20, and S21). The porosity of π-X was first examined by CO_2 adsorption experiment. The CO_2 adsorption isotherms show that π-PY, π-Nap, and π-Ph display similar CO_2 adsorption capacities of about 8.0 $cm^3\ g^{-1}$ at 298 K and 1 atm (Figure S22). Moreover, the I_2 adsorption experiments of π-X were performed to further characterize the pore characteristics by soaking π-X in an *n*-hexane solution of I_2. As shown in Figures 2c, S23, and S24, the intensities of UV–vis characteristic absorption peaks of I_2 at approximately 526 nm gradually decrease along with the increased soaking time, which nearly disappear at 8 h for the three π-X frameworks [43, 44]. These results suggest that π-PY, π-Nap, and π-Ph possess similar pore characteristic.

The optical absorption properties of π-X were investigated by solid-state UV–vis-NIR spectra. As shown in Figure 2d, all π-X samples exhibit strong light-harvesting ability from UV to NIR region. The band gap energies (E_g) of π-PY, π-Nap, and π-Ph are evaluated by the Kubelka–Munk (KM) method, which are 1.89, 1.80, and 1.93 eV, respectively (Figures S25–S27). Moreover, the valence band x-ray photoelectron spectroscopy (XPS) of π-PY, π-Nap, and π-Ph were performed to determine their valence band (VB) positions [45, 46]. As shown in Figures S28–S30, the VB potentials of π-PY, π-Nap, and π-Ph are 0.75, 0.96, and 0.90 V versus NHE, respectively. Therefore, the conduction band (CB) potentials of π-PY, π-Nap, and π-Ph are accordingly calculated to be −1.14, −0.84, and −1.03 V versus NHE, respectively, based on the equation of $E_g = E_{VB} - E_{CB}$ (Figure S31) [47–50]. From a thermodynamic perspective, the photogenerated electrons of π-X frameworks can easily transfer to other co-catalysts to achieve photocatalytic reactions due to their negative CB potentials [51, 52].

Encouraged by the above analysis, the photocatalytic CO_2 reduction experiments of π-X were conducted in pure H_2O reaction medium and >99% CO_2 atmosphere with dinuclear cobalt complex (Co_2L) as the co-catalyst (Figure S32) [53], benzyl alcohol as the electron donor, and in the absence of any additional noble-metal photosensitizers. Under visible light irradiation, π-X exhibit high catalytic performance for the photoreduction of CO_2 to $HCOO^-$. As shown in Figure S33, the $HCOO^-$ production rates of π-PY, π-Nap, and π-Ph are 6749, 5048, and 2183 μmol $g^{-1}\ h^{-1}$, respectively. Notably, π-PY with the most π–π stacking interactions exhibits the highest photocatalytic activity for $HCOO^-$ production among the three π-X samples, demonstrating that π–π stacking interactions plays a critical role in improving catalytic performance for CO_2 photoreduction. Moreover, no other reduction product except $HCOO^-$ was detected in the catalytic systems, indicating that the $HCOO^-$ selectivities of all π-X samples are nearly 100%.

Given that π-X exhibit outstanding light-harvesting ability in the NIR region, the NIR-light-driven CO_2 reduction experiments of

15213773, 0, Downloaded from https://onlinelibrary.wiley.com/doi/10.1002/anie.7481604 by Tianjin University Of Technology, Wiley Online Library on [29/05/2026]. See the Terms and Conditions (https://onlinelibrary.wiley.com/terms-and-conditions) on Wiley Online Library for rules of use; OA articles are governed by the applicable Creative Commons License

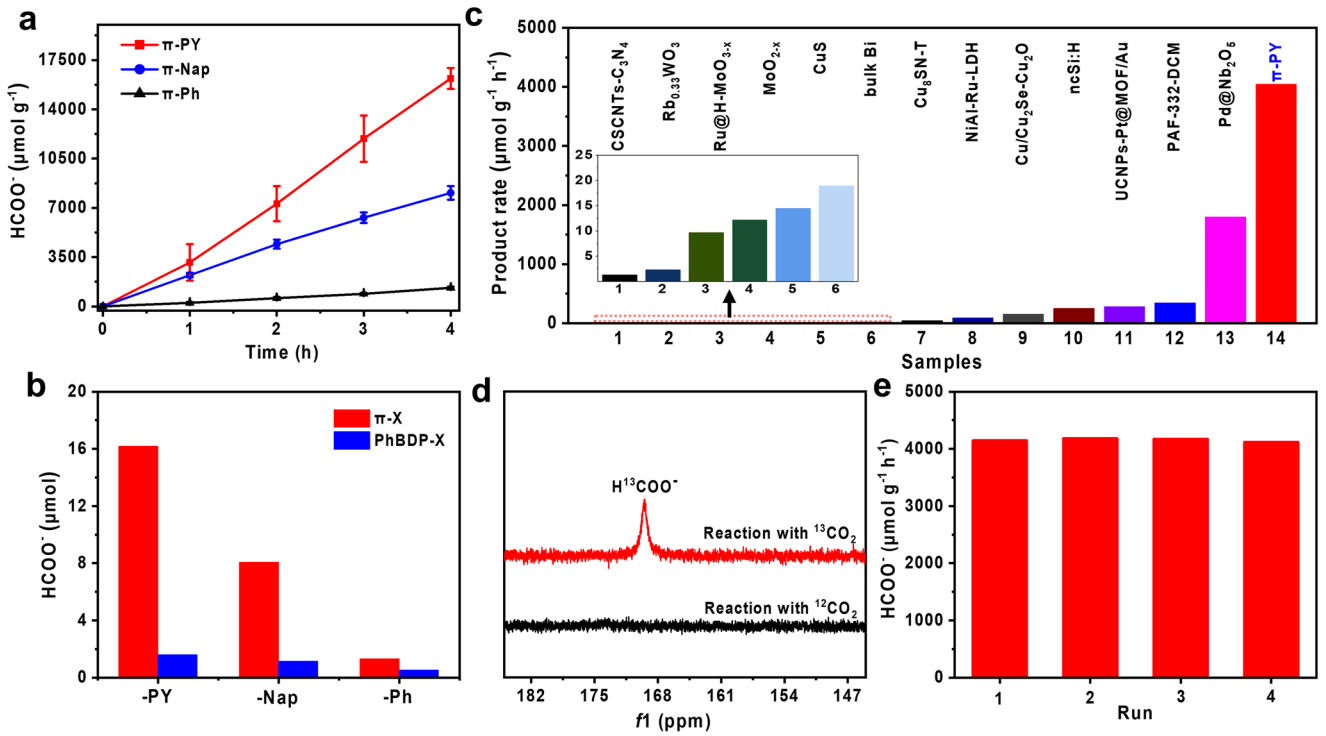

FIGURE 3 | (a) The amounts of $HCOO^-$ produced over π-X under NIR light irradiation and in >99% CO_2 atmosphere. (b) The $HCOO^-$ Yields of π-X and PhBDP-X under NIR light irradiation. (c) Performance comparison of π-PY and the reported photocatalysts for NIR-light-driven CO_2 reduction without additional noble-metal photosensitizers. (d) ^{13}C NMR spectra of the liquid product generated from the photocatalytic CO_2 reduction over π-PY using $^{13}CO_2$ instead of $^{12}CO_2$. (e) The photocatalytic $HCOO^-$ production rate of π-PY in four consecutive runs.

π-X were further carried out. As shown in Figure 3a, the π-X with different π–π stacking interactions also exhibit significantly different catalytic activities for CO_2 photoreduction to $HCOO^-$ under NIR light irradiation, among which π-PY achieves the highest $HCOO^-$ production rate of 4045 μmol g^{-1} h^{-1} ($HCOO^-$ selectivity, ~100%), which is ca. 2 and 12 times higher than those of π-Nap and π-Ph, respectively. Furthermore, the benzaldehyde was detected by ^1H NMR spectrum in the catalytic system. The molar ratios of benzaldehyde and $HCOO^-$/HCOOH are all close to 1:1 for π-X, implying that the electrons generated through benzyl alcohol oxidation are all used to CO_2 reduction (Figures S34–S36) [54, 55]. Moreover, a large number of small-sized single crystals of π-X can be also obtained when the dichloromethane solution of PhBDP-X was evaporated for 3 h. Taking π-PY as a representative example, the powder XRD pattern and catalytic performance of the small-sized single crystals are basically equivalent to those of the large-sized single crystals, indicating that we can efficiently obtain π–π stacked photocatalysts by changing the synthetic method (Figures S37–S39). In addition, the photocatalytic CO_2 reduction experiments over π-PY were conducted using TEOA, EtOH, and BuOH (1-butanol) as sacrificial electron donors under identical conditions. The results demonstrate that π-PY exhibited appreciable $HCOO^-$ generation rates, which are slightly lower than that obtained with benzyl alcohol. These results confirm the general applicability of the system across different sacrificial donors (Figure S40).

The homogeneous photocatalytic experiments over PhBDP-X (X = PY, Nap, and Ph) were evaluated in CH_3CN/H_2O (v:v = 4:1) reaction medium under NIR light irradiation with Co_2L as the co-catalyst, benzyl alcohol as the electron donor, and without any additional noble-metal photosensitizers. After 4 h of light irradiation, the $HCOO^-$ yields of PhBDP-PY, PhBDP-Nap, and PhBDP-Ph are 1.60, 1.14, and 0.52 μmol, respectively (Figure 3b). It is worth noting that the $HCOO^-$ yields over π-X are significantly higher than those of PhBDP-X, demonstrating that π–π stacking plays a critical role in improving photocatalytic performance (Figure 3b). Moreover, taking π-PY as a representative example, it also exhibits significantly higher photocatalytic performance than that of amorphous PhBDP-PY powders for CO_2 photoreduction to $HCOO^-$ (Figures S41 and S42). To elucidate their different catalytic performance, we measured photocurrent response and analyzed the rise/decay time constants of photocurrent response. π-PY possesses obviously higher photocurrent response and shows the faster rise time (τ_{rise} = 0.31 s) and the slower decay (τ_{decay} = 2.9 s) than those of amorphous PhBDP-PY powders, demonstrating that the π–π stacking structure effectively promotes the separation and transport of photogenerated charge carriers (Figure S43). All these results indicate that the much-enhanced photocatalytic activity for CO_2 reduction can be attributed to the growing π–π stacking interactions, which can serve as an electron-transfer channel to facilitate photo-induced electron delivery [34]. To the best of our knowledge, the catalytic activity of π-PY is higher than most of the reported photocatalytic systems under similar reaction conditions (Figure 3c and Table S3).

A series of control experiments over π-PY have been carried out, no CO_2 reduction product was detected in the absence of CO_2, Co_2L, NIR light irradiation, or benzyl alcohol, demonstrating that all these factors are indispensable for the NIR-light-driven

15213773, 0, Downloaded from https://onlinelibrary.wiley.com/doi/10.1002/anie.7481604 by Tianjin University Of Technology, Wiley Online Library on [29/05/2026]. See the Terms and Conditions (https://onlinelibrary.wiley.com/terms-and-conditions) on Wiley Online Library for rules of use; OA articles are governed by the applicable Creative Commons License

CO_2 reduction reaction (Figure S44). Under NIR light irradiation, the actual photothermal temperature of the reaction system was measured to be 45°C. To rigorously exclude any contribution from photothermal effects and to confirm that the observed catalytic activity is genuinely driven by photoexcitation rather than thermal effects, a slightly higher temperature (50°C) was chosen for the dark control experiment. The result shows that no CO_2 reduction product over π-PY was detected under dark conditions, confirming that the photocatalytic activity indeed originates from light excitation rather than thermal effects (Figures S44 and S45). Moreover, the $HCOO^-$ production rate over π-PY obviously increases with the enhancement of the light intensity of the NIR light (Figure S46). Collectively, these control experiments provide robust evidence that NIR irradiation contributes to charge carrier (electrons and holes) generation in π-PY, and the concentration of charge carrier increases along with the increased light intensity of the NIR light. Therefore, in NIR-light-driven CO_2 reduction, NIR irradiation enables effective activation of the catalyst to generate electrons and holes; π–π stacking enhances charge separation efficiency and facilitates electrons delivery; the synergy between the two factors leads to high catalytic efficiency of π-PY.

The isotope trace experiment of CO_2 reduction by π-PY was carried out, where the CO_2 was replaced with $^{13}CO_2$, to verify the carbon source of $HCOO^-$. As shown in Figure 3d, a distinct characteristic signal appears at 169.5 ppm in the ^{13}C NMR spectrum, which can be assigned to $H^{13}COO^-$, verifying that $HCOO^-$ is indeed derived from the NIR-light-driven CO_2 reduction [56]. Furthermore, the catalytic durability of π-PY for NIR-light-driven CO_2 reduction was evaluated by successive cycle experiments. The $HCOO^-$ generation rates keep almost unchanged after four consecutive cycles, indicative of the really excellent photocatalytic stability of π-PY (Figure 3e). In addition, powder XRD patterns show the structural integrity of π-X after photocatalytic reaction, unveiling their excellent structural stability (Figures S47–S49).

The photocurrent response, electrochemical impedance spectroscopy (EIS), photoluminescence (PL) emission, and time-resolved PL (TRPL) spectra of π-X were tested to study charge separation and transfer efficiencies, as well as to illustrate the higher photocatalytic activity of π-PY compared with π-Nap and π-Ph. As shown in Figure 4a, all π-X samples exhibit obvious photocurrent signals, among which the π-PY possesses the highest photocurrent response. Moreover, π-PY shows the fastest rise time ($\tau_{rise} = 0.31$ s) and the slowest decay ($\tau_{decay} = 2.9$ s) (Table S4) [57]. These results suggest that π-PY exhibits the best charge separation and fastest electron transfer. The results of EIS show that π-PY displays a smaller semicircle radius than π-Nap and π-Ph (Figure 4b). Furthermore, the results of the Nyquist plots fitting indicating that π-PY possesses smaller R_{ct} value (14.1 kΩ) than π-Nap (17.4 kΩ) and π-Ph (31.4 kΩ) [58, 59]. These results imply that π-PY shows the smallest charge-transfer resistance, supporting its fastest electron transfer. In the PL spectra analysis, π-PY shows the weakest emission intensity among the three π-X samples, indicating that it possesses the most efficient charge separation (Figure 4c). Furthermore, the results of TRPL spectra demonstrate that the average lifetime of π-PY is 0.9 ns, which is smaller than those of π-Nap (1.21 ns) and π-Ph (1.66 ns), further verifying that π-PY displays the most efficient charge separation (Figure 4d) [60]. In addition, we have performed transient absorption (TA) spectroscopy of π-PY, π-Nap, and π-Ph to directly probe the electron transfer kinetics. The results demonstrate that π-PY shows the shortest excited-state lifetime among the three π frameworks, corresponding to the fastest charge transfer rate, which effectively increases the probability of charge carriers participating in CO_2 reduction (Figures S50–S53) [61]. All the above results reveal that the growing π–π stacking interactions in π-X frameworks can increase charge separation and transfer efficiency, and prolong carrier lifetime, among which the π-PY with the most π–π stacking interactions exhibits the most efficient charge separation, fastest electron transfer and longest carrier lifetime, thereby explaining its highest catalytic activity for CO_2 photoreduction.

Additionally, the photocatalytic CO_2 reduction by π-X in low CO_2 concentration (15% CO_2 and 85% N_2) was further studied. It was found that π-X also exhibits excellent catalytic activities for the CO_2 photoreduction to $HCOO^-$. Under visible light irradiation, the $HCOO^-$ generation rates of π-PY, π-Nap, and π-Ph are 2548, 768, and 408 μmol g^{-1} h^{-1}, respectively (Figure S54). Moreover, under NIR light irradiation, π-PY, π-Nap, and π-Ph still exhibit excellent photocatalytic performance for CO_2 reduction, with the $HCOO^-$ generation rates of 1693, 569, and 189 μmol g^{-1} h^{-1}, respectively (Figure S55). No other reduction product was detected in both reaction conditions, demonstrating that the $HCOO^-$ selectivity is nearly 100%. These results show again that the catalytic activity of π frameworks for CO_2 photoreduction can be improved by growing π–π stacking interactions. It is worth noting that the photocatalytic performance of π-PY for low-concentration CO_2 photoreduction is also superior to most of the reported photocatalysts under similar reaction conditions (Table S5).

A possible mechanism for the photocatalytic CO_2 reduction to $HCOO^-$ over π-PY/Co_2L system was investigated. As shown in Figure 5a, the cyclic voltammogram (CV) of π-PY shows a reduction wave at −1.35 V versus NHE, which is more negative than that of Co_2L (−0.97 V vs. NHE), demonstrating that the thermodynamic feasibility for photogenerated electrons transfer from π-PY to Co_2L [62]. Moreover, in situ XPS measurements of π-PY/Co_2L under dark and light were conducted. In the dark, π-PY/Co_2L shows Co $2p_{3/2}$ and Co $2p_{1/2}$ binding energies at 781.64 and 797.41 eV, respectively, which exhibit negative shift to 781.35 and 797.10 eV, respectively, upon light irradiation, suggesting that Co^{II} accepts electrons (Figure 5b). Thus, the possible mechanism was proposed: upon NIR light irradiation, π-PY is excited to produce electrons and holes, in which the electrons are transferred rapidly to the surface of the π-PY by π–π stacking, which are further transferred to Co_2L co-catalyst to reduce Co^{II} to produce Co^{I}. The generated Co^{I} reduces the adsorbed CO_2 to generate $HCOO^-$, and photogenerated holes of π-PY oxidize benzyl alcohol to benzaldehyde (Figure S56). For homogeneous photocatalytic systems, taking PhBDP-PY as a representative example, the quenched mode of the excited state [PhBDP-PY]* can be assigned to a reductively quenched mechanism, which was confirmed by fluorescence quenching experiments (Figures S57 and S58) [63]. Upon NIR illumination, the [PhBDP-PY] is excited to produce excited state [PhBDP-PY]*, which is quenched by benzyl alcohol via electron transfer to form the reduced $[PhBDP\text{-}PY]^{\bullet-}$, and benzyl alcohol was oxidized to benzaldehyde. Subsequently, $[PhBDP\text{-}PY]^{\bullet-}$ transfers

15213773, 0, Downloaded from https://onlinelibrary.wiley.com/doi/10.1002/anie.7481604 by Tianjin University Of Technology, Wiley Online Library on [29/05/2026]. See the Terms and Conditions (https://onlinelibrary.wiley.com/terms-and-conditions) on Wiley Online Library for rules of use; OA articles are governed by the applicable Creative Commons License

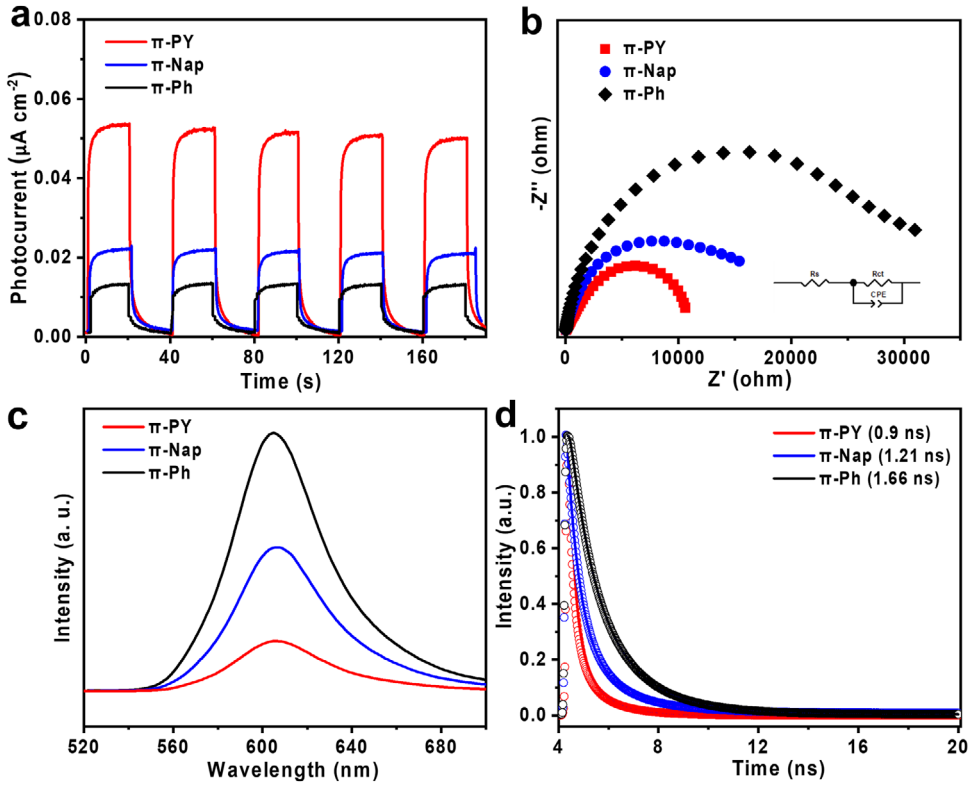

FIGURE 4 | (a) Photocurrent response of π-X. (b) EIS spectra of π-X. (c) PL spectra of π-X. (d) TRPL of π-X.

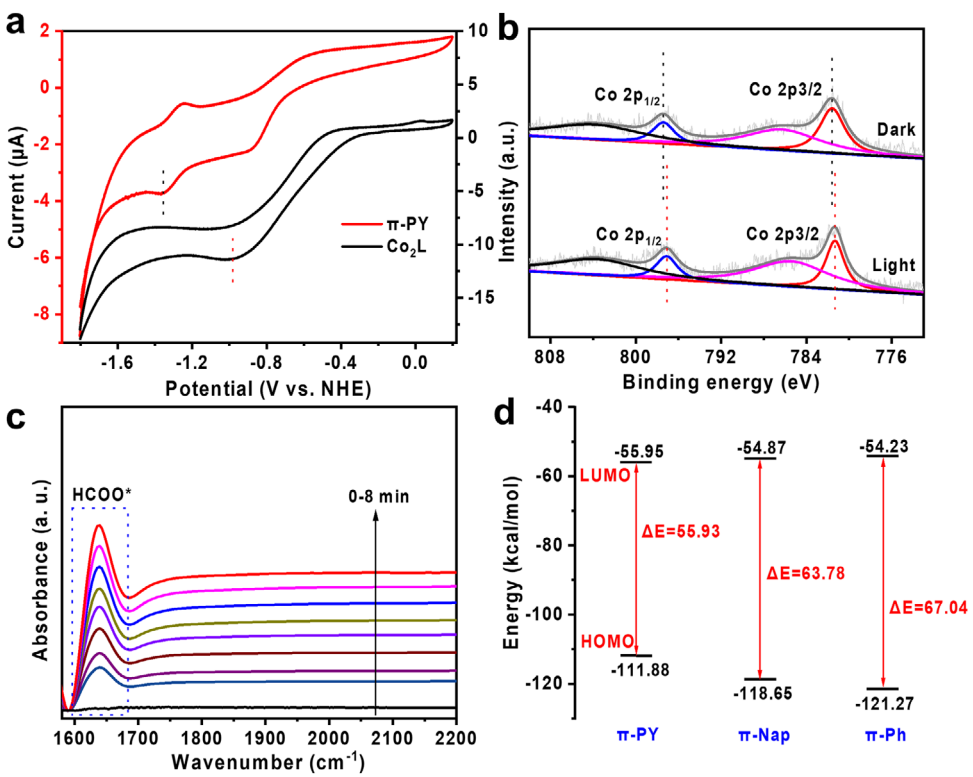

FIGURE 5 | (a) CV curves of π-PY and Co_2L. (b) XPS spectra of Co in the dark and under light irradiation for π-PY/Co_2L. (c) In situ FTIR spectra of π-PY/Co_2L. (d) Energy gaps between HOMO and LUMO of π-PY, π-Nap, and π-Ph.

15213773, 0, Downloaded from https://onlinelibrary.wiley.com/doi/10.1002/anie.7481604 by Tianjin University Of Technology, Wiley Online Library on [29/05/2026]. See the Terms and Conditions (https://onlinelibrary.wiley.com/terms-and-conditions) on Wiley Online Library for rules of use; OA articles are governed by the applicable Creative Commons License

electrons to the Co_2L co-catalyst to reduce Co^{II} to produce Co^{I} and regenerating the ground-state [PhBDP-PY]. Finally, the generated Co^{I} reduces the adsorbed CO_2 to generate $HCOO^-$ (Figure S59). In order to monitor the key intermediates in the process of CO_2 photoreduction to $HCOO^-$, in situ Fourier transform infrared (FTIR) measurements of π-PY/Co_2L during CO_2 reduction were carried out. As shown in Figure 5c, a new adsorption peak at 1641 cm^{-1} was detected, which can be assignable to the HCOO*, the key intermediate for CO_2 photoreduction to $HCOO^-$. The intensity of this peak gradually increases with increasing illumination time, suggesting the incremental concentration of HCOO* intermediate for CO_2 photoreduction [64].

Density functional theory (DFT) calculations were performed to further elucidate the significantly enhanced photocatalytic CO_2 reduction activity of π-PY compared with π-Nap and π-Ph. Four PhBDP-X structural units were stacked together by π–π stacking interactions, which were picked out for model building to calculate the energy gaps of highest occupied molecular orbital (HOMO)-lowest unoccupied molecular orbital (LUMO). As shown in Figures 5d and S60–S62, the energy gaps between HOMO and LUMO of π-PY, π-Nap, and π-Ph are 55.93, 63.78, and 67.04 kcal mol^{-1}, respectively. Obviously, π-PY shows the lowest energy gap, which is most favorable for electron transfer among the three π-X frameworks [65]. The calculated results are in good agreement with those of experimental results, thereby explaining again the highest catalytic activity of π-PY for CO_2 photoreduction to $HCOO^-$ among the three π-X frameworks.

3 | Conclusion

In summary, by modulating conjugated aromatic moieties, three new π frameworks with different π–π stacking interactions have been rationally designed and synthesized for NIR-light-driven CO_2 reduction. Among them, the π-PY with the most π–π stacking interactions exhibits the highest catalytic activity for CO_2 photoreduction to $HCOO^-$ coupled with benzyl alcohol oxidation to benzaldehyde using dinuclear cobalt complex as the co-catalyst. The $HCOO^-$ generation rate of π-PY is 4045 μmol g^{-1} h^{-1}, which is 2 and 12 times higher than those of π-Nap and π-Ph. Furthermore, π-PY also exhibits a splendid catalytic activity for NIR-light-driven low-concentration CO_2 reduction, with $HCOO^-$ production rate of 1693 μmol g^{-1} h^{-1}. To our knowledge, the catalytic performance of π-PY are superior to most of the reported photocatalytic systems under similar reaction conditions. Systematic studies demonstrate that such high photocatalytic activity of π-PY is attributed to its abundant π–π stacking interactions, which not only facilitates charge separation and transfer, but also prolongs carrier lifetime and lowers the energy gap between HOMO and LUMO. This work provides a facile approach for improving catalytic performance of NIR-light-driven CO_2 reduction.

Author Contributions

Chong-Jiu Lu: investigation, writing – original draft. **Xin-Yue Zheng**: investigation. **Yun-Nan Gong**: writing – original draft, writing – review and editing, formal analysis. **Di-Chang Zhong**: supervision, writing – review and editing, project administration. **Tong-Bu Lu**: methodology.

Acknowledgments

This work was supported by the National Key R&D Program of China (2022YFA1502902), the National Natural Science Foundation of China (22571228, 22371208, 22271218, and 22531007), and the Natural Science Foundation of Tianjin City (24JCZDJC00220 and 24JCYBJC00800).

Conflicts of Interest

The authors declare no conflicts of interest.

Data Availability Statement

The data that supports the findings of this study are available in the Supporting Information of this article.

References

1. D. Shindell and C. J. Smith, "Climate and Air-Quality Benefits of a Realistic Phase-Out of Fossil Fuels," *Nature* 573 (2019): 408–411, https://doi.org/10.1038/s41586-019-1554-z.

2. Q.-X. Zhou, Y. Guo, and Y.-F. Zhu, "Reticular Copper Dual Sites Embedded With Semiconductor Particles for Selective CO_2-to-C_2H_4 Photoreduction," *Nature Catalysis* 8 (2025): 728–739, https://doi.org/10.1038/s41929-025-01369-8.

3. R.-B. Lin and B. Chen, "Reducing CO_2 With Stable Covalent Organic Frameworks," *Joule* 2 (2018): 1030–1032, https://doi.org/10.1016/j.joule.2018.05.017.

4. J.-Y. Ye, N. Dimitratos, L. M. Rossi, N. Thonemann, A. M. Beale, and R. Wojcieszak, "Too Much of a Good Thing: Lessons From Compromised Rootworm Bt Maize in the US Corn Belt," *Science* 387 (2025): 6737, https://doi.org/10.1126/science.adm7634.

5. K. Sun, Y.-Y. Qian, and H.-L. Jiang, "Metal–Organic Frameworks for Photocatalytic Water Splitting and CO_2 Reduction," *Angewandte Chemie International Edition* 62 (2023): e202217565; *Angewandte Chemie* 135 (2023): e202217565, https://doi.org/10.1002/anie.202217565.

6. P. Fratzl, "Introduction: Sustainable Materials," *Chemical Reviews* 123 (2023): 1841–1842, https://doi.org/10.1021/acs.chemrev.3c00091.

7. J.-Y. Weng, M. Yue, Q. Li, et al., "3D Interpenetrated Covalent Organic Frameworks," *Coordination Chemistry Reviews* 535 (2025): 216614, https://doi.org/10.1016/j.ccr.2025.216614.

8. J. Chen, R. Abazari, K. A. Adegoke, et al., "Metal–Organic Frameworks and Derived Materials as Photocatalysts for Water Splitting and Carbon Dioxide Reduction," *Coordination Chemistry Reviews* 469 (2022): 214664, https://doi.org/10.1016/j.ccr.2022.214664.

9. Y.-N. Gong, X. Guan, and H.-L. Jiang, "Covalent Organic Frameworks for Photocatalysis: Synthesis, Structural Features, Fundamentals and Performance," *Coordination Chemistry Reviews* 475 (2023): 214889, https://doi.org/10.1016/j.ccr.2022.214889.

10. L. Zhang, J. Liu, and Y.-Q. Lan, "New Frontier in Artificial Photosynthesis," *Accounts of Chemical Research* 57 (2024): 870–883, https://doi.org/10.1021/acs.accounts.3c00751.

11. Y.-Q. Zhang, P. Li, P. Cui, et al., "Precisely Constructing Molecular Junctions in Hydrogen-Bonded Organic Frameworks for Efficient Artificial Photosynthetic CO_2 Reduction," *Angewandte Chemie International Edition* 63 (2024): e202413131; *Angewandte Chemie* 136 (2024): e202413131, https://doi.org/10.1002/anie.202413131.

12. T. Wakabayashi, Y. Kametani, E. Tanahashi, et al., "Ferrocenyl PNNP Ligands-Controlled Chromium Complex-Catalyzed Photocatalytic Reduction of CO_2 to Formic Acid," *Journal of the American Chemical Society* 146 (2024): 25963–25975, https://doi.org/10.1021/jacs.4c03683.

13. Y. Wang, J.-X. Wei, H.-L. Tang, et al., "Artificial Photosynthetic System for Diluted CO_2 Reduction in Gas-Solid Phase," *Nature Communications* 15 (2024): 8818, https://doi.org/10.1038/s41467-024-53066-y.

15213773, 0, Downloaded from https://onlinelibrary.wiley.com/doi/10.1002/anie.748160d by Tianjin University Of Technology, Wiley Online Library on [29/05/2026]. See the Terms and Conditions (https://onlinelibrary.wiley.com/terms-and-conditions) on Wiley Online Library for rules of use; OA articles are governed by the applicable Creative Commons License

14. Q. Li, J.-N. Chang, Z.-M. Wang, et al., "Modulated Connection Modes of Redox Units in Molecular Junction Covalent Organic Frameworks for Artificial Photosynthetic Overall Reaction," *Journal of the American Chemical Society* 145 (2023): 23167–23175, https://doi.org/10.1021/jacs.3c07471.

15. S.-X. Zhou, Y.-X. Kuang, H.-S. Yang, et al., "Structure-Controlled Interpenetrated MOF@COF Via C−C Linkage for Enhanced Photocatalysis," *Angewandte Chemie International Edition* 63 (2024): e202412279; *Angewandte Chemie* 136 (2024): e202412279, https://doi.org/10.1002/anie.202412279.

16. J.-H. Ding, X.-Y. Guan, J. Lv, et al., "Three-Dimensional Covalent Organic Frameworks With Ultra-Large Pores for Highly Efficient Photocatalysis," *Journal of the American Chemical Society* 145 (2023): 3248–3254, https://doi.org/10.1021/jacs.2c13817.

17. W.-L. Wang, C.-L. Ji, K. Liu, C.-G. Zhao, W.-P. Li, and J. Xie, "Dinuclear Gold Catalysis," *Chemical Society Reviews* 50 (2021): 1874–1912, https://doi.org/10.1039/D0CS00254B.

18. Y. Xu, J.-P. Dong, L. Wang, et al., "3D Cluster-Based Covalent Organic Framework for Efficient CO_2 Photoreduction," *Angewandte Chemie International Edition* 64 (2025): e202501391; *Angewandte Chemie* 137 (2025): e202501391, https://doi.org/10.1002/anie.202501391.

19. D.-S. Zhang, L. Wang, X.-D. Zhang, et al., "Emerging Inorganic–Organic Hybrid Photocatalysts for Solar-Driven Overall Water Splitting: Progress and Perspectives," *Chemical Society Reviews* 54 (2025): 9978–10005, https://doi.org/10.1039/D5CS00378D.

20. J.-W. Wang and G.-F. Ouyang, "Designing Interactions Between Molecular Catalysts and Light Absorbers for Fine-Tuned Performances and Electron-Transfer Mechanisms in CO_2 Photoreduction," *Accounts of Chemical Research* 58 (2025): 2862–2874, https://doi.org/10.1021/acs.accounts.5c00456.

21. C.-Y. Hu, X. Chen, J.-X. Low, et al., "Near-Infrared-Featured Broadband CO_2 Reduction With Water to Hydrocarbons by Surface Plasmon," *Nature Communications* 14 (2023): 221, https://doi.org/10.1038/s41467-023-35860-2.

22. Z.-H. Wang, C. Cao, L. Jiang, Z.-H. Xing, J.-T. Jia, and G.-S. Zhu, "Near-Infrared Light Catalysis of Carbon Dioxide Reduction by Conjugated Porous Aromatic Frameworks," *Angewandte Chemie International Edition* 64 (2025): e202508924; *Angewandte Chemie* 137 (2025): e202508924, https://doi.org/10.1002/anie.202508924.

23. S.-C. Song, C.-C. Xin, W. Liu, et al., "Near-Infrared Light-Driven CO_2 Reduction on Cup-Stacked Carbon Nanotubes," *Angewandte Chemie International Edition* 64 (2025): e202415173; *Angewandte Chemie* 137 (2025), e202415173.

24. S.-Q. Li, Z.-X. Li, J.-N. Yue, et al., "Photocatalytic CO_2 Reduction by Near-Infrared-Light (1200 nm) Irradiation and a Ruthenium-Intercalated NiAl-Layered Double Hydroxide," *Angewandte Chemie International Edition* 63 (2024): e202407638; *Angewandte Chemie* 136 (2024), e202407638, https://doi.org/10.1002/anie.202407638.

25. L.-B. Jiang, J.-J. Yang, S.-Y. Zhou, et al., "Strategies to Extend Near-Infrared Light Harvest of Polymer Carbon Nitride Photocatalysts," *Coordination Chemistry Reviews* 439 (2021): 213947, https://doi.org/10.1016/j.ccr.2021.213947.

26. C. Sun, J.-L. Yin, and H.-H. Fei, "Highly Stable π-Extended Viologen Functionalized Hybrid Lead Halides for Near Infrared-Driven CO_2-to-C_2H_4 Photoconversion," *Angewandte Chemie International Edition* 64 (2025): e202514206; *Angewandte Chemie* 137 (2025): e202514206.

27. S.-H. Yang, W. Che, Y.-H. Shao, et al., "Advancements and Prospects of Near-Infrared-Light Driven CO_2 Reduction Reaction," *Chemical Society Reviews* 54 (2025): 7174–7215, https://doi.org/10.1039/D4CS00721B.

28. N. T. La Porte, J. F. Martinez, S. Chaudhuri, S. Hedstrom, V. S. Batista, and M. R. Wasielewski, "Photoexcited Radical Anion Super-Reductants for Solar Fuels Catalysis," *Coordination Chemistry Reviews* 361 (2018): 98–119, https://doi.org/10.1016/j.ccr.2018.01.018.

29. J. Li, X.-L. Liu, X. Wu, et al., "Selective CO_2 Photoreduction Into CH_4 Triggered by the Synergy Between Oxygen Vacancy and Ru Substitution Under Near-Infrared Light Irradiation," *Advancement of Science* 11 (2024): 2405668, https://doi.org/10.1002/advs.202405668.

30. X. Wu, W.-L. Zhang, J. Li, Q.-J. Xiang, Z.-Y. Liu, and B. Liu, "Identification of the Active Sites on Metallic MoO_2^- X Nano-Sea-Urchin for Atmospheric CO_2 Photoreduction under UV, Visible, and Near-Infrared Light Illumination," *Angewandte Chemie International Edition* 62 (2023): e202213124; *Angewandte Chemie* 135 (2023): e202213124, https://doi.org/10.1002/anie.202213124.

31. J. Li, W.-F. Pan, Q.-Y. Liu, et al., "Interfacial Engineering of $Bi_{19}Br_3S_{27}$ Nanowires Promotes Metallic Photocatalytic CO_2 Reduction Activity Under Near-Infrared Light Irradiation," *Journal of the American Chemical Society* 143 (2021): 6551–6559, https://doi.org/10.1021/jacs.1c01109.

32. X.-Y. Wu, Y. Li, G.-K. Zhang, et al., "Photocatalytic CO_2 Conversion of $M_{0.33}WO_3$ Directly From the Air With High Selectivity: Insight Into Full Spectrum-Induced Reaction Mechanism," *Journal of the American Chemical Society* 141 (2019): 5267–5274, https://doi.org/10.1021/jacs.8b12928.

33. B. Wang, H.-L. Chen, W. Zhang, et al., "Semimetallic Bismuthene With Edge-Rich Dangling Bonds: Broad-Spectrum-Driven and Edge-Confined Electron Enhancement Boosting CO_2 Hydrogenation Reduction," *Advanced Materials* 36 (2024): 2312676, https://doi.org/10.1002/adma.202312676.

34. J.-H. Mei, Y.-R. Zeng, Y.-N. Gong, W.-J. Shi, D.-C. Zhong, and T.-B. Lu, "π–π Stacking as Electron-Transfer Channels in Hydrogen-Bonded Organic Frameworks for Boosting Photocatalysis," *Angewandte Chemie International Edition* 64 (2025): e202507332; *Angewandte Chemie* 137 (2025), e202507332, https://doi.org/10.1002/anie.202507332.

35. Y.-L. Ma, D.-D. Cai, S. Wan, et al., "Control Over π-π Stacking of Heteroheptacene-Based Nonfullerene Acceptors for 16% Efficiency Polymer Solar Cells," *National Science Review* 7 (2020): 1886–1895, https://doi.org/10.1093/nsr/nwaa189.

36. L.-X. Qiao, S. R. Pena, M. Martínez-Ibanez, et al., "Anion π–π Stacking for Improved Lithium Transport in Polymer Electrolytes," *Journal of the American Chemical Society* 144 (2022): 9806–9816, https://doi.org/10.1021/jacs.2c02260.

37. Y. Yao, X.-Y. Zhang, Y.-Y. Cao, L. Liu, Y.-Q. Zhang, and S.-J. Zhang, "Single-Site Pd Regulated by π–π Stacking for High-Selectivity Cyclopropanation Reaction," *Journal of the American Chemical Society* 146 (2024): 31053–31061, https://doi.org/10.1021/jacs.4c10860.

38. Z.-L. Zhang, X. Hu, S. Qiu, et al., "Boron–Nitrogen-Embedded Polycyclic Aromatic Hydrocarbon-Based Controllable Hierarchical Self-Assemblies through Synergistic Cation–π and C–H···π Interactions for Bifunctional Photo- and Electro-Catalysis," *Journal of the American Chemical Society* 146 (2024): 11328–11341.

39. K. U. Do, A. V. Conner, and S. E. Wheeler, "Making Sense of Heteroatom Effects in π–π Interactions," *Journal of the American Chemical Society* 147 (2025): 32273–32286, https://doi.org/10.1021/jacs.5c12769.

40. J.-H. Zhang, Y.-N. Gong, H.-J. Wang, et al., "Ordered Heterogeneity of Molecular Photosensitizer Toward Enhanced Photocatalysis," *Proceedings National Academy of Science USA* 119 (2022): e2118278119, https://doi.org/10.1073/pnas.2118278119.

41. J.-H. Mei, S. Lai, Y.-N. Gong, et al., "A Supramolecular-Nanocage-Based Framework Stabilized by π–π Stacking Interactions With Enhanced Photocatalysis," *Angewandte Chemie International Edition* 64 (2025): e202413413; *Angewandte Chemie* 137 (2025), e202413413, https://doi.org/10.1002/anie.202413413.

42. C. Bonnier, D. D. Machin, O. Abdi, and B. D. Koivisto, "The Challenges of Using 2,6-Disubstituted BODIPY Cores Within Donor–Acceptor Light-Harvesting Motifs," *Organic & Biomolecular Chemistry* 11 (2013): 3756–3760, https://doi.org/10.1039/c3ob40213d.

43. X.-R. Zhang, J. Maddock, T. M. Nenoff, M. A. Denecke, S.-H. Yang, and M. Schroder, "Adsorption of Iodine in Metal–Organic Framework

15213773, 0, Downloaded from https://onlinelibrary.wiley.com/doi/10.1002/anie.74816O4 by Tianjin University Of Technology, Wiley Online Library on [29/05/2026]. See the Terms and Conditions (https://onlinelibrary.wiley.com/terms-and-conditions) on Wiley Online Library for rules of use; OA articles are governed by the applicable Creative Commons License

Materials," *Chemical Society Reviews* 51 (2022): 3243–3262, https://doi.org/10.1039/D0CS01192D.

44. N.-Y. Huang, H. He, S.-J. Liu, et al., "Electrostatic Attraction-Driven Assembly of a Metal–Organic Framework With a Photosensitizer Boosts Photocatalytic CO_2 Reduction to CO," *Journal of the American Chemical Society* 143 (2021): 17424–17430, https://doi.org/10.1021/jacs.1c05839.

45. H.-Q. Wang, E. Altman, C. Broadbridge, Y.-M. Zhu, and V. Henrich, "Determination of Electronic Structure of Oxide–Oxide Interfaces by Photoemission Spectroscopy," *Advanced Materials* 22 (2010): 2950–2956, https://doi.org/10.1002/adma.200903759.

46. T. Hellmann, C. Das, T. Abzieher, et al., "The Electronic Structure of MAPI-Based Perovskite Solar Cells: Detailed Band Diagram Determination by Photoemission Spectroscopy Comparing Classical and Inverted Device Stacks," *Advanced Energy Materials* 10 (2020): 2002129, https://doi.org/10.1002/aenm.202002129.

47. Q.-X. Zhou, Y. Guo, and Y.-F. Zhu, "Photocatalytic Sacrificial H_2 Evolution Dominated by Micropore-Confined Exciton Transfer in Hydrogen-bonded Organic Frameworks," *Natural Catastrophe* 6 (2023): 574–584, https://doi.org/10.1038/s41929-023-00972-x.

48. R.-K. Liu, D. Zhao, S.-L. Ji, et al., "Harvesting Singlet and Triplet Excitation Energies in Covalent Organic Frameworks for Highly Efficient Photocatalysis," *Nature Materials* 24 (2025): 1245–1257, https://doi.org/10.1038/s41563-025-02281-z.

49. G.-X. Lan, Y.-J. Fan, W.-J. Shi, E. You, S. S. Veroneau, and W.-B. Lin, "Biomimetic Active Sites on Monolayered Metal–Organic Frameworks for Artificial Photosynthesis," *Natural Catastrophe* 5 (2022): 1006–1018, https://doi.org/10.1038/s41929-022-00865-5.

50. S.-S. Li, C.-M. Gao, H.-H. Yu, et al., "Vinylene-Linked Donor-π-Acceptor Metal–Covalent Organic Framework for Enhanced Photocatalytic CO_2 Reduction," *Angewandte Chemie International Edition* 63 (2024): e202409925; *Angewandte Chemie* 136 (2024): e202409925, https://doi.org/10.1002/anie.202409925.

51. H. Miyabe and S. Kohtani, "Photocatalytic Single Electron Transfer Reactions on TiO_2 Semiconductor," *Science China Chemistry* 62 (2019): 1439–1449, https://doi.org/10.1007/s11426-019-9626-9.

52. Y.-F. Liu, T. Handa, N. Olsen, C. Nuckolls, and X.-Y. Zhu, "Spin-Polarized Charge Separation at Two-Dimensional Semiconductor/Molecule Interfaces," *Journal of the American Chemical Society* 146 (2024): 10052–10059, https://doi.org/10.1021/jacs.4c00956.

53. Y.-N. Gong, S.-Q. Zhao, H.-J. Wang, et al., "A Planar-Structured Dinuclear Cobalt(II) Complex With Indirect Synergy for Photocatalytic CO_2-to-CO Conversion," *Angewandte Chemie International Edition* 63 (2024): e202411639; *Angewandte Chemie* 136 (2024): e202411639.

54. B. Lei, G. Zhou, Z. Gong, et al., "Dynamically Cyclic Fe^{2+}/Fe^{3+} Active Sites as Electron and Proton-Feeding Centers Boosting CO_2 Photoreduction Powered by Benzyl Alcohol Oxidation," *Research* 8 (2025): 0567, https://doi.org/10.34133/research.0567.

55. G. Cheng, W. Zhang, A. Jentys, et al., "Importance of Interface Open Circuit Potential on Aqueous Hydrogenolytic Reduction of Benzyl Alcohol Over Pd/C," *Nature Communications* 13 (2022): 7967, https://doi.org/10.1038/s41467-022-35554-1.

56. H.-Q. Xu, J. Hu, D. Wang, et al., "Visible-Light Photoreduction of CO_2 in a Metal–Organic Framework: Boosting Electron–Hole Separation Via Electron Trap States," *Journal of the American Chemical Society* 137 (2015): 13440–13443, https://doi.org/10.1021/jacs.5b08773.

57. Y.-H. Cho, M.-Y. Yang, J.-Y. Cui, et al., "Analysis of the TiO_2 Photoanode Process Using Intensity Modulated Photocurrent Spectroscopy and Distribution of Relaxation Times," *Journal of the American Chemical Society* 147 (2025): 7703–7710, https://doi.org/10.1021/jacs.4c17345.

58. Z.-G. Zhou, L.-H. Li, B.-L. Li, et al., "N-Heterocyclic Olefin Type Ionic Liquid With Innate Soft Lewis-Base Character as an Effective Additive for Hybrid Quasi-2D and 3D Perovskite Solar Cells," *Small* 19 (2023): 2300013, https://doi.org/10.1002/smll.202300013.

59. W.-T. Li, B. Han, Y.-H. Liu, et al., "Unsymmetric Protonation Driven Highly Efficient H_2O_2 Photosynthesis in Supramolecular Photocatalysts Via One-Step Two-Electron Oxygen Reduction," *Angewandte Chemie International Edition* 64 (2024): e202421356; *Angewandte Chemie* 137 (2024): e202421356.

60. B. Wang, R. He, L.-H. Xie, et al., "Microporous Hydrogen-Bonded Organic Framework for Highly Efficient Turn-Up Fluorescent Sensing of Aniline," *Journal of the American Chemical Society* 142 (2020): 12478–12485, https://doi.org/10.1021/jacs.0c05277.

61. F. Xu, Y. He, J. Zhang, G. Liang, C. Liu, and J. Yu, "Prolonging Charge Carrier Lifetime via Intraband Defect Levels in S-Scheme Heterojunctions for Artificial Photosynthesis," *Angewandte Chemie International Edition* 64 (2025): e202414672; *Angewandte Chemie* 137 (2025), e202414672.

62. P. Wang, S. Guo, H.-J. Wang, et al., "A Broadband and Strong Visible-Light-Absorbing Photosensitizer Boosts Hydrogen Evolution," *Nature Communications* 10 (2019): 3155, https://doi.org/10.1038/s41467-019-11099-8.

63. B. Pinto-Pacheco, W. P. Carbery, S. Khan, D. B. Turner, and D. Buccella, "Fluorescence Quenching Effects of Tetrazines and Their Diels–Alder Products: Mechanistic Insight Toward Fluorogenic Efficiency," *Angewandte Chemie International Edition* 59 (2020): 22140–22149; *Angewandte Chemie* 132 (2020): 22326–22335.

64. Z.-F. Zhao, Y.-L. Zheng, C. Wang, et al., "Fabrication of Robust Covalent Organic Frameworks for Enhanced Visible-Light-Driven H_2 Evolution," *ACS Catalysis* 11 (2021): 2098–2107, https://doi.org/10.1021/acscatal.0c04820.

65. Q. Wang, Q. Zhang, Q.-W. Zhang, et al., "Color-Tunable Single-Fluorophore Supramolecular System With Assembly-Encoded Emission," *Nature Communications* 11 (2020): 158, https://doi.org/10.1038/s41467-019-13994-6.

Supporting Information

Additional supporting information can be found online in the Supporting Information section.

Supporting File 1: anie72610-sup-0001-SuppMat.docx.

Supporting File 2: anie72610-sup-0002-cif.zip.

15213773, 0, Downloaded from https://onlinelibrary.wiley.com/doi/10.1002/anie.74816O4 by Tianjin University Of Technology, Wiley Online Library on [29/05/2026]. See the Terms and Conditions (https://onlinelibrary.wiley.com/terms-and-conditions) on Wiley Online Library for rules of use; OA articles are governed by the applicable Creative Commons License